Korean J. Chem. Eng., 38(4), 852-861 (2021)
DOI: 10.1007/s11814-020-0671-6

pISSN: 0256-1115
eISSN: 1975-7220

Solubility of ethylene in N-methyl-2-pyrrolidone: Experimental study and estimation of UNIQUAC activity model parameters

Mohammad Yousefi, Shima Azizi†, Seyed Mohsen Peyghambarzadeh, and Zoha Azizi

Department of Chemical Engineering, Mahshahr Branch, Islamic Azad University, Mahshahr, Iran
(*Received 10 July 2020 • Revised 29 August 2020 • Accepted 1 September 2020*)

Abstract−The solubility of ethylene in N-methyl-2-pyrrolidone (NMP) was evaluated at different temperatures, including 278.2, 298.2, and 328.2 K, and different pressures in an experimental pressure decaying setup. The kinetic and equilibrium results were obtained for pure gas absorption. Henry's law constants were calculated at different temperatures. Eventually, thermodynamic modeling was done using Peng Robinson equation of state (PR-EOS) and UNIQUAC activity coefficient model. The binary interaction parameters, τ_{12}, τ_{21}, were adjusted and optimized. Regarding the values obtained for binary interaction parameters, it was concluded that this solution has non-ideal behavior. Indeed, because of its low prediction error (3-11%), it was concluded that the correlated thermodynamic model could accurately predict the experimental data.

Keywords: Absorption, Ethylene, NMP, Peng Robinson, Solubility, UNIQUAC

INTRODUCTION

Pivotal feedstock for engineering resins and plastics are light olefins, such as ethylene, so their industrial production is very important. Ethylene can be achieved in the industrial cracking process because it is not naturally present in crude oil and natural gas. Most of the time, approximately equal proportions of mixtures of olefins and paraffins are found in the mixture of cracked off-gas. Due to their similarity in physicochemical properties, these olefins and paraffins are hardly separated from each other. For example, the kinetic diameters of ethylene and ethane are 0.375 and 0.385 nm, respectively, whereas their boiling points are about 169 K and 184 K. The main current process for olefins and paraffins separation is cryogenic distillation. It is a highly energy-intensive process because severe operating conditions, including low temperatures (183-258 K) and high pressures (7-28 bar), exist in that separation [1-7]. Several alternative processes, such as extractive distillation, membrane and adsorption technology, have also been suggested. However, these superseded technologies are hardly utilized commercially because of possible feed contamination or regeneration [4-6,8-10]. Absorption is another ethylene separation method in which a proper selective solvent such as polyethylene [11], ionic liquids [12,13], methyl propionate [14], toluene [15,16], norbornene [15], Cucl/Aniline/N-methylpyrrolidone [8], and aqueous silver nitrate [17] could be applied to separate ethylene from its containing mixture.

In addition to experimental solubility studies, researchers investigated the thermodynamic modeling of absorption of gases in solvents at a wide range of pressures and temperatures with different thermodynamic models in order to obtain their optimal parameters [6].

†To whom correspondence should be addressed.
E-mail: s.azizi.chem@gmail.com

Chemlar et al. [11] used a gravimetric apparatus to measure ethylene solubility in 13 polyethylene samples at temperature from 333 to 423 K. To evaluate the solubility, they used swelling corrections based on the experimental data and considered temperature dependent crystallinities.

Shariati et al. [14] measured the solubility of ethylene in methyl propionate by experimental methods and modeling with Peng-Robinson equation of state within a temperature range of 283.5-464.8 K and pressure up to 107 bar with an accuracy of 5.8%.

Sato et al. [15] investigated the solubility of ethylene in toluene, norbornene and toluene/norbornene mixtures at temperatures of 323, 343, and 363 K, and at pressures up to 57 bar. The Peng-Robinson equation of state could correlate the experimental solubility in binary and ternary systems with the prediction error of about 3%.

Dojcansky et al. [18] measured the P-x data for mixtures of hexane/cyclohexane, hexane/benzene/cyclohexane, hexane/cyclohexane/N-methylpyrrolidone, and hexane/benzene/N-methylpyrrolidone at 343 K. Then, with the help of Wilson activity model, VLE for the multicomponent mixtures were predicted.

Lee et al. [16] measured the solubility of ethylene in toluene from 323 to 423 K, and pressure range from 5 to 25 bars using pressure decaying method. The experimental solubility data were correlated by the bubble-pressure calculation with the Peng-Robinson equation of state incorporated with the van der Waals one-fluid and Zhong-Masuoka mixing rules with the consideration of binary interaction parameters.

Nagahama et al. [19] predicted VLE of five ternary systems at one atmosphere, such as acetone-benzene-chloroform and methyl acetate-benzene-cyclohexane using the Wilson activity model parameters determined from the binary data.

Cancelas et al. [20] studied the solubility and diffusivity of propylene, ethylene, and propylene-ethylene mixture in polypropylene at different temperature and pressure. They used Sanchez-Lacombe EOS to obtain isothermal absorption of both binary systems. For

both systems, binary interaction parameters decreased with temperature.

Kumar and Mondal [21] studied the equilibrium solubility of carbon dioxide in aqueous binary mixture of 2-(Diethylamino)ethanol (DEEA) and 1,6-hexamethyldiamine (HMDA) in the temperature range of 303-333 K and inlet partial pressure of 10.1-20.3 kPa and at different concentrations in semi-batch operated laboratory scale bubble column.

Dashti et al. [22] estimated the solubility of hydrogen sulfide in ionic liquid ([bmim][PF_6]) using molecular dynamics simulation technique as well as artificial intelligence knowledge of hybrid genetic algorithm-adaptive neuro fuzzy inference system (GA-ANFIS) and an empirical polynomial regression (PR) model.

Kitagishi et al. [23] measured the solubility and diffusivity of ethylene in four propylene-based copolymer (cPP) samples at below and above melting point temperatures of each sample. These values were achieved with cPP crystallinity and free-volume-theory (FVT) parameters found from molten state data.

Mi et al. [24] investigated absorption of ethylene from ethane/ethylene mixture with $AgNO_3$ solution in ultrasonic microreactor. They evaluated the effect of ultrasound on absorption, mass transfer coefficient and bubble size reduction. Stronger absorption was observed in the presence of ultrasound in this system.

In this work, an in-depth in vitro study was performed on the solubility of ethylene in NMP solvent in the range of 278.2 to 328.2 K and pressure up to 14 bars. In addition to the kinetic and equilibrium results of absorption, a thermodynamic modeling was performed using PR EOS-UNIQUAC activity coefficient model to find the solubility and optimize the binary interaction parameters. Finally, the accuracy of the calculations was determined by comparing the experimental and the model results.

EXPERIMENTAL

1. Materials

High purity ethylene gas (C_2H_4) and NMP solvent (C_5H_9NO) were supplied from Amir Kabir Petrochemical Company (AKPC), Mahshahr, Iran. Ethylene purity was 99.8 mol.% and NMP solvent purity was about 99.7 wt%. None of the chemicals used needed further purification. Given the high boiling point (475.15 K) and low vapor pressure of the NMP solvent (0.0007 bar at 298.15 K compared with 0.032 bar for water) compared to other industrial solvents, the probability of solvent loss during the process was assumed to be negligible. This solvent is dissolved in water, smells close to amine, and is a transparent liquid. This solvent produced by the German company, BASF, contained minor amounts of dimethyl pyrrolidone, water, mono methyl amine, butyric lactone. According to the analysis, maximum 1 mol.% of water was present in the solvent. The NMP solvent solubilizes unsaturated hydrocarbons more than saturated hydrocarbons [4]. This property, coupled with the high polarity and solubility of this solvent, makes it a good choice for separating olefins from paraffins. The chemical structure of NMP solvent and ethylene gas can be seen in Fig. 1.

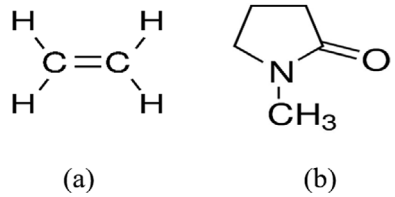

Fig. 1. The chemical structure of (a) ethylene (b) NMP.

Table 1. The properties of the materials used in this study [25,26]

Component	T_c (K)	P_c (bar)	ω	M_w (g/mol)	A	B	C
Ethylene	282.35	50.418	0.0866	28.054	6.96636	649.806	262.73
NMP	724	47.2	0.361	99.13	7.36115	1,869.62	215.294

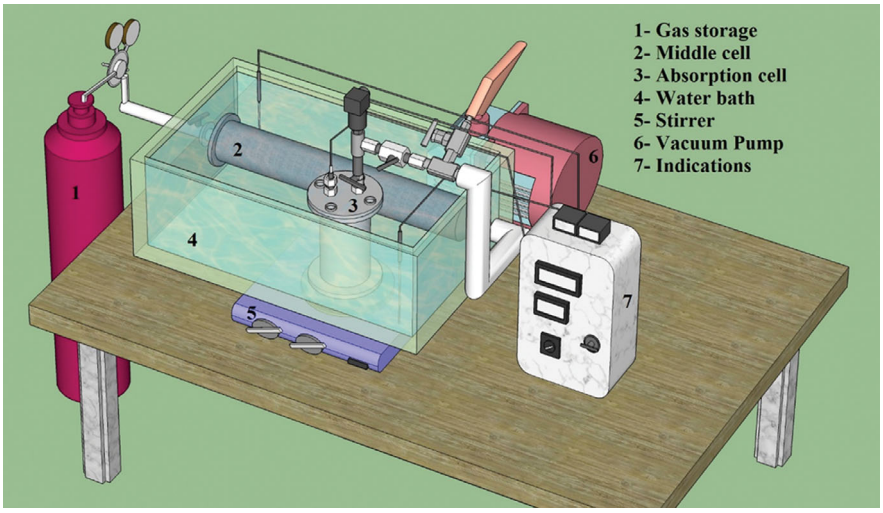

Fig. 2. Schematic representation of the experimental apparatus.

The Antoine equation ($\log P^{sat}$ (mmHg)=$A-\frac{B}{T(^{\circ}C)+C}$) is used to calculate these components vapor pressure. The coefficients of this equation along with the critical properties of ethylene and NMP are presented in Table 1.

2. Apparatus

In this study, the solubility experiments were continued until the solvent became completely saturated with the gas. It is the equilibrium condition at which no pressure change occurs. The experimental apparatus is a batch pressure decaying absorption device. The temperature setting of this setup is controlled manually by a water bath equipped with PT-100Ω as a temperature sensor.

As shown in Fig. 2, the gas absorption in the NMP solvent was carried out in an absorption cell equipped with a magnetic stirrer. Gas storage tank, regulator, middle or intermediate cell, absorption or equilibrium cell, magnetic stirrer, vacuum pump, water bath, pressure and temperature transmitters, and some indicators are components of this setup.

For each test, the required amount of solvent (about 100 ml) was poured into the absorption cell and the lid was tightened. Then, using the vacuum pump (JB Industries DV-200N, USA), the air was completely discharged from this setup. After ensuring complete evacuation, the valve between the intermediate cell and equilibrium cell was closed. The ethylene feed gas could now be directed from the storage tank to the middle cell. This cell is 500 ml in volume with 200 bar pressure tolerance and made of stainless steel. The purpose of the intermediate cell is to regulate the temperature and pressure of the gas before it enters the absorption cell. Using the intermediate cell initial pressure, the total amount of the initial moles of the injected gas can be calculated. After making sure the temperature and pressure were adjusted in the middle cell, it was necessary to open the valve between the middle cell and the absorption cell to begin the absorption. Due to the sudden increase in volume, the pressure dropped sharply and stabilized in an instant. Then, the pressure reduction continued slowly to reach the equilibrium. In all these experiments, pressure changes were recorded by time.

The equilibrium cell was equipped with a temperature RTD sensor (PT-100Ω) with an accuracy of ±0.2 K, and absolute pressure transducer (model PSCH0025BCIJ of Sensys Co.) with a precision of ±0.01 bar. The volume of this cell and its connections, which were equipped with a magnetic stirrer, was 370 ml. The equilibrium cell was able to withstand pressure up to 25 bar. The magnetic stirrer speed should be adjusted to increase heat and mass transfer rate as well as to reduce the time to reach the equilibrium. Note that a vortex should not be created on the surface of the solvent inside the absorption cell, while thorough mixing should also be performed. The temperature and pressure measured in this are displayed by digital indicators.

It was ensured that no leakage occurred during the absorption process. The accuracy and performance of the instruments (RTD and pressure transducer) were also ensured. The accurate volume of the total media including the absorption cell, intermediate cell, and all connections and tubing was measured with a precision of ±3 ml. This setup has been used in past researches [6,27-30], and the obtained results have been approved by different approaches.

3. Assumptions and Calculations

Important assumptions in calculating the mole fraction or gas solubility in the absorption experiments are as follows:

1. Due to the lack of volatility of NMP solvent during the experiments, no solvent enters the gas phase, and therefore, it is assumed to have pure gas phase.

2. After evacuating, the amount of air remaining in the equilibrium cell can be assumed to be negligible.

3. Because the gas phase is pure, the mass transfer resistance in the gas phase can be neglected.

4. During the absorption, no volume change was observed in the solvent. The solubility of ethylene gas in NMP solvent is very low (x<0.1), and this small solubility cannot change the solvent volume significantly.

The volume of gas in the absorption cell can be calculated from the difference between the total volume of the cell and the volume of the solvent:

$$V_{g,f}=V_t-V_s \tag{1}$$

where V_s is the initial volume of the solvent, V_t is total volume of the cell, and $V_{g,f}$ is the final volume of the gas.

At constant temperature and constant volume of the solvent, a mass balance from initial pressure to equilibrium pressure must be established for relating the initial moles of the gas with the final moles of the gas in the system to obtain the moles of gas absorbed in the solvent.

$$n_g=\frac{1}{RT}\left[\frac{P_1\cdot V_{g,1}}{Z_1}-\frac{P_{eq}\cdot V_{g,f}}{Z_{eq}}\right] \tag{2}$$

where $V_{g,1}$ is the initial volume of the gas (intermediate cell volume), $V_{g,f}$ is the final volume of the gas (intermediate and equilibrium cell volume), R is gas constant (83.14 bar·cm^3/mol·K), T is the operating temperature (K), P_1 is the initial pressure (bar), P_{eq} is the final or equilibrium pressure (bar), Z_1 is compressibility factor at the initial condition, and Z_{eq} is compressibility factor at the equilibrium condition. The compressibility factor was calculated using Peng Robinson EOS [31,32].

The number of moles of solvent can be calculated as follows:

$$n_s=\frac{\rho_s\cdot V_s}{M_s} \tag{3}$$

where ρ_s is density of the solvent (g/cm^3), V_s is the solvent volume, and M_s is the molecular weight of the solvent.

Finally, the solubility was calculated by dividing the moles of the absorbed gas into the sum of the moles of the absorbed gas and the moles of the solvent:

$$x=\frac{n_g}{n_g+n_s} \tag{4}$$

where x is mole fraction of the gas in the solvent (solubility), n_g is moles of the absorbed gas and n_s is moles of the solvent. The uncertainty analysis of mole fraction was performed and presented in the Supplementary Information. According to the results obtained, the maximum uncertainty of x was 5.2%.

In addition, Henry's law constants were calculated from the solubility data using the slope of the equilibrium pressure versus sol-

ubility at each temperature when the intercept of the straight line was considered zero. Pressure variation versus solubility should be considered linear if Henry's law is established.

According to Eq. (5), the relation between equilibrium pressure and solubility of dilute solution is expressed as:

$$P_{eq} = K_H \times x \tag{5}$$

where K_H is Henry's law constant.

In accordance with the Arrhenius model, Henry's law constant can be correlated with temperature as Eq. (6):

$$K_H = H_0 \exp\left(\frac{-E}{RT}\right) \tag{6}$$

A plot of $\ln K_H$ in terms of the inverse of temperature gives a straight line whose slope and intercept provide values of ΔH (=R×slope) and ΔS (=−R×intercept) and the parameter of the Arrhenius equation.

Finally, the Gibbs free energy value was calculated according to Eq. (7):

$$\Delta G = \Delta H - T\Delta S \tag{7}$$

THERMODYNAMIC MODELING

For modeling and calculating the VLE, the Φ-γ approach was used as follows [25]:

$$y_1 \Phi_1 P = x_1 \gamma_1 P_1^{sat} \tag{8}$$

where y_1 is mole fraction of ethylene in the gas phase, x_1 is mole fraction of ethylene in the liquid phase, P is total pressure (or equilibrium pressure), Φ_1 is fugacity coefficient of ethylene in the gas phase, γ_1 is activity coefficient of ethylene in the liquid phase, and P_1^{sat} is saturated pressure of ethylene.

According to Eqs. (9)-(16), the values of compressibility factor and Φ were calculated from PR EOS [31-36]. According to the above assumptions, the gas phase can be assumed to be pure (y_1=1), because the solvent volatility is negligible [6,30]. With this assumption, there was no need to apply the mixing rules of PR EOS. The value of fugacity coefficient was calculated using Eq. (9):

$$\ln \Phi = Z - 1 - \ln(Z - B) - \frac{A}{2\sqrt{2}B} \ln\left(\frac{Z + 2.414B}{Z - 0.414B}\right) \tag{9}$$

where Z was calculated using PR-EOS as follows:

$$Z^3 - (1-B)Z^2 + (A - 2B - 3B^2)Z - (AB - B^2 - B^3) = 0 \tag{10}$$

The terms A and B and their associated parameters were calculated as follows:

$$A = \frac{aP}{R^2T^2} \tag{11}$$

$$B = \frac{bP}{RT} \tag{12}$$

$$b = 0.077796 \frac{RT_c}{P_c} \tag{13}$$

$$m = 0.37464 + 1.54226\omega - 0.26992\omega^2 \tag{14}$$

$$\alpha = [1 + m(1 - T_r^{0.5})]^2 \tag{15}$$

$$a = 0.457235 \frac{R^2 T_c^2}{P_c} \alpha \tag{16}$$

where T_c is critical temperature (K), P_c is critical pressure (bar), ω is acentric factor, T_r is reduced temperature, Φ is fugacity coefficient, and Z is compressibility factor.

In this study, the UNIQUAC activity coefficient model was used to calculate γ. As can be seen in Eq. (17), this model contains two different parts, including combinational and residual. The combinational part is related to the entropy contribution and the residual is to the intermolecular forces involved in the enthalpy of mixing. The combinational part is determined only by the composition, size, and shape of the molecules and requires only pure data. The residual depends on the intermolecular forces and, therefore, the adjustable binary interaction parameters, τ_{12} and τ_{21}, appear only in this part. These parameters always are greater than zero. The UNIQUAC activity coefficient model for the binary system is given by Eqs. (17)-(25) [25,37-41]:

$$\ln \gamma_i = \ln \gamma_i^C + \ln \gamma_i^R \tag{17}$$

$$\ln \gamma_i^C = \ln \frac{\Phi_i}{x_i} + 5q_i \ln \frac{\theta_i}{\Phi_i} + l_i - \frac{\Phi_i}{x_i} \Sigma_j x_j l_j \tag{18}$$

$$\ln \gamma_i^R = q_i \left(1 - \ln(\Sigma_j \theta_j \tau_{ji}) - \Sigma_j \frac{\theta_j \tau_{ij}}{\Sigma_k \theta_k \tau_{kj}}\right) \tag{19}$$

$$\tau_{ij} = \exp\left(-\frac{u_{ij} - u_{ii}}{RT}\right) = \exp\left(-\frac{a_{ij}}{T}\right) \tag{20}$$

$$l_i = 5(r_i - q_i) - (r_i - 1) \tag{21}$$

$$\Phi_i = \frac{x_i r_i}{\Sigma_j x_j r_j} \tag{22}$$

$$\theta_i = \frac{x_i q_i}{\Sigma_j x_j q_j} \tag{23}$$

$$r_i = \Sigma_k v_k^{(i)} R_k \tag{24}$$

$$q_i = \Sigma_k v_k^{(i)} Q_k \tag{25}$$

where r and q are molecular structure constants of the pure component and depend on the relative molecular size (volume) and the relative molecular surface area, respectively. Each of them is given, respectively, by the sum of the parameters R and Q of the functional groups comprising the compounds. In the above equa-

Table 2. Essential parameters for the UNIQUAC model in this work [40]

i	Name	Main group	k	j	R_k	Q_k	$v_k^{(i)}$
1	Ethylene (CH_2=CH_2)	1	2	1	0.6744	0.54	2
2	NMP	44	85	2	3.981	3.2	1

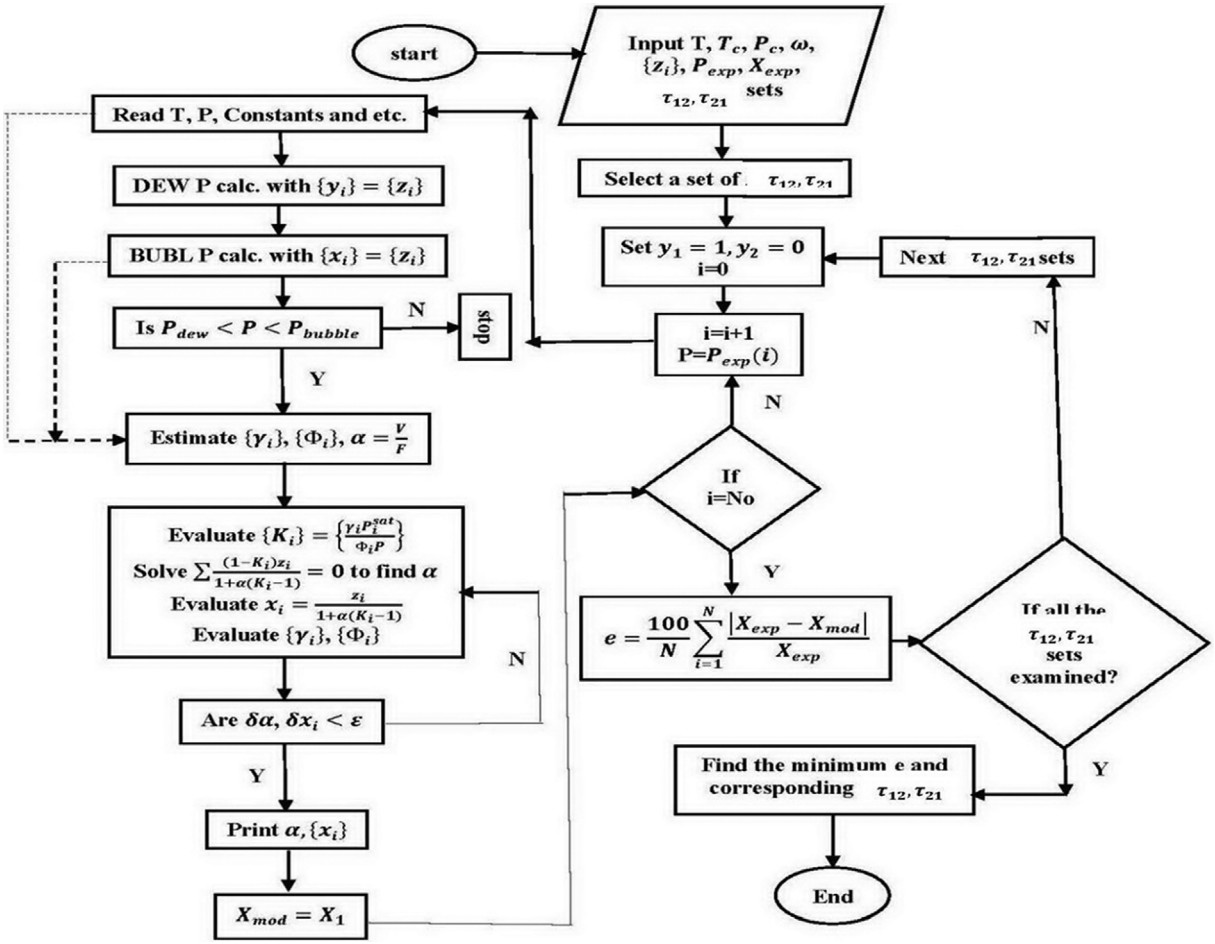

Fig. 3. The algorithm used to calculate the solubility of ethylene in NMP based on PR-EOS and UNIQUAC activity coefficient model.

tions, i represents the components and j and k are the dummy indices. In these equations, θ_i is a function of the surface, and Φ_i is a function of the volume. The parameters needed for these equations for the ethylene-NMP system can be seen in the Table 2.

The algorithm for calculating the liquid mole fraction as well as the optimization of the binary interaction parameters from the experimental solubility data is shown in Fig. 3. Based on this flowchart, the binary interaction parameters are adjusted so that the least error in the prediction of the solubility results is obtained. The required data and constants were taken as input and then a set of binary interaction parameters were selected. By choosing each experimental pressure, a flash calculation was performed using the Φ-γ approach. As a result, the solubility values of the model (x_{model}) were obtained. When the solubility results were calculated using any set of binary interaction parameters and all pressures at constant temperature, then, the absolute average deviation (A.A.D.) was calculated according to the following equation based on the solubility values to optimize and adjust the binary interaction parameters.

$$\%AAD = \frac{100}{N}\Sigma_{i=1}^{N}\frac{|x_{exp} - x_{mod}|}{x_{exp}} \quad (26)$$

where x_{exp} is the experimental mole fraction and x_{mod} is the mole fraction from model prediction.

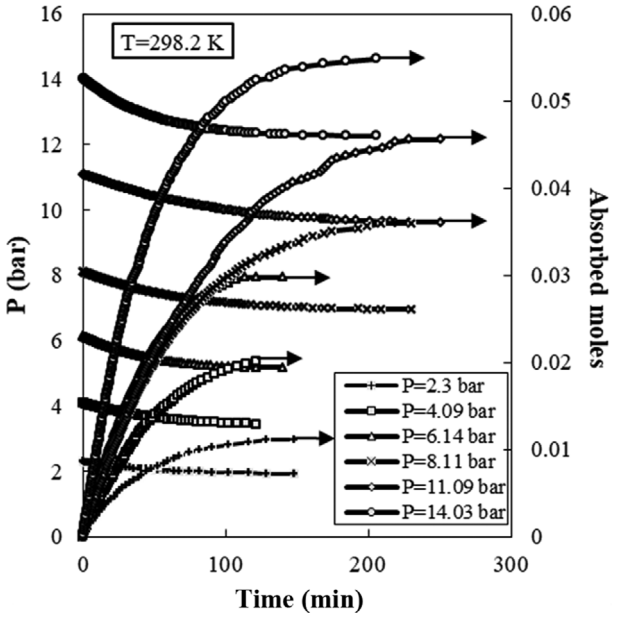

Fig. 4. Time dependence of the pressure decay and the absorbed moles of ethylene in NMP at 298.2 K and different initial pressures.

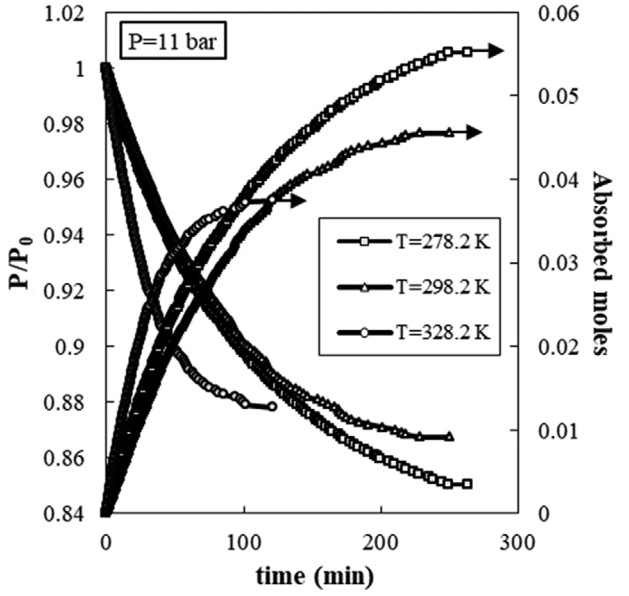

Fig. 5. Time dependence of the pressure decay and the absorbed moles of ethylene in NMP at about 11 bar and various temperatures.

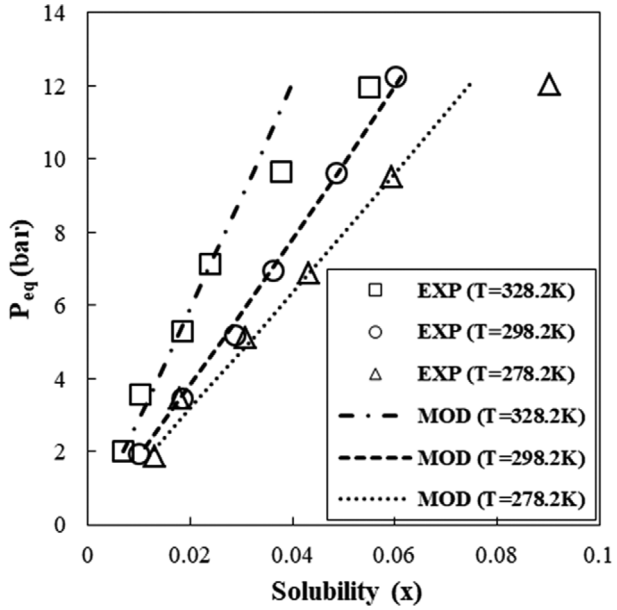

Fig. 6. The equilibrium data and the model prediction for the absorption of ethylene in NMP at different temperatures.

RESULTS AND DISCUSSION

1. Kinetics of Absorption

Fig. 4 demonstrates the pressure decay and amounts of absorbed moles versus time for ethylene absorption in NMP at constant temperature of 298.2 K and different initial pressures. Similar graphs were obtained for other temperatures (278.2 and 328.2 K), which are not shown here. The total experimental time for this system was recorded at all pressures and temperatures from 80 to 260 minutes to attain equilibrium.

Note that the pressure drop during the test will continue until the solvent is saturated with the gas. In fact, after reaching the final pressure, the pressure drop is no longer observed and equilibrium pressure is achieved. According to the initial contract for all the experiments, if no pressure drop was observed within 20 minutes, that pressure was considered as the equilibrium pressure. According to these graphs, the higher the initial pressure, the higher the pressure decay, and the better the absorption rate.

Also, Fig. 4 shows the amounts of absorbed moles of ethylene along time at different initial pressures. It is clear that when the absorption is conducted at higher pressures, more time is needed to reach the equilibrium and hence, more amount of ethylene gas was absorbed in the solvent.

Fig. 5 shows the variation of pressure and absorbed moles with time at constant pressure (about 11 bars) and at different temperatures, respectively. Similar graphs were also drawn for other initial pressures and different temperatures. From these graphs, it can be concluded that at lower temperatures and constant pressure, more absorption is observed and more time is needed to reach the equilibrium.

The higher the temperature, the faster the absorption rate. This point is obvious from the initial slope of the P/P_0 curves in Fig. 5. According to Fig. 5, the initial slope of these curves at temperatures of 278.2, 298.2 and 328.2 K are about 0.00063, 0.00065 and 0.00129, respectively, which confirms this point. Also in Fig. 5, the initial slope of the absorbed moles curves increased with increasing temperature and confirmed faster absorption at higher temperatures. The values of this initial slope are 0.00022, 0.00023 and 0.00039, respectively.

2. Absorption Equilibrium

The equilibrium mole fraction of ethylene gas in NMP solvent was calculated using Eq. (4). Fig. 6 presents the equilibrium data of this system at constant temperatures of 278.2, 298.2 and 328.2 K. In this figure, the results of model prediction of the equilibrium solubility are also presented, which indicates a small difference between the model results and the experimental data. The modelling results will be discussed in the next section.

Fig. 6 shows that increase in temperature decreases ethylene equilibrium solubility. At higher pressure, the effect of temperature on the solubility was more significant.

According to Eqs. (5) and (6), the slope of the equilibrium pressure versus solubility graph gives the constant of Henry's law K_H for each temperature. Henry's law constant is calculated at each temperature because it is a function of temperature only. Henry's law can be used when the partial pressure is between 5 to 10 bar and the solubility is less than about 3 mol.% [37]. For this reason, only those data (in Fig. 6) which were at these ranges of pressure and solubility (infinite dilution) were used to calculate Henry's law constants. According to Fig. 7, by plotting $\ln K_K$ versus inverse of temperature, Arrhenius model constants are obtained using experimental solubility data. These data are also shown in Table 3.

In fact, the activation energy ($\Delta H = -E$) indicates the temperature dependence of absorption. Higher activation energy reveals that the solvent absorption capacity would be greater when the temperature increases. According to Svenssons et al. [42], the ab-

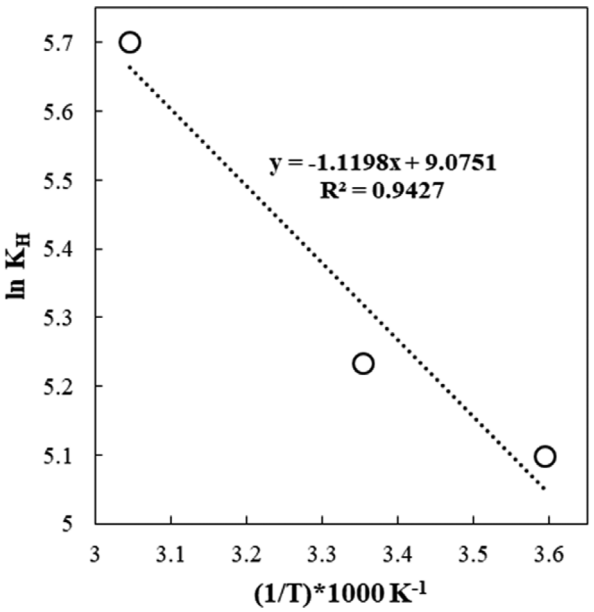

Fig. 7. The Arrhenius type model to calculate Henry's law constant as a function of temperature.

sorption enthalpy of less than 14-16 kJ/mol indicates physical absorption. Based on the heat of absorption presented in Table 3, the ethylene solubility in NMP is intrinsically physical and occurs during low energy exchange absorption.

The calculated Henry's law constants and also the constants of the Arrhenius equation for ethylene/NMP/water system were compared with the scarce previous works in Table 3. Comparison of the results of other researches with this work showed that the results of this research were close to them.

Since there was a probability of a very small amount of water in the solvent (x_w=0.011), and by comparing this work with others [43,44] it was evident that with increasing water content in the NMP solvent, Henry's law constant increases and eventually the solubility of the gas in the solvent decreases. It is also evident that the increase in temperature increased Henry's law constant.

According to the results of Table 3, due to the negative heat of absorption, the absorption process is exothermic. As can be seen from the results, at any experimental temperature the value of |TΔS| is higher than the |ΔH| value, i.e., the absorption is more affected by the decreased irregularity than the absorption energy. Also, as the temperature increases, |TΔS|/|ΔH| increases. This case shows that at higher temperatures, the entropy effects more than the enthalpy effects affect the Gibbs free energy and absorption process. Increasing the temperature decreases the system's irregularity. The positive Gibbs free energy also indicates the non-spontaneous absorption process. As the temperature increases, the Gibbs free energy increases further (its value gets more positive). This is precisely because of the greater effect of entropy on Gibbs free energy with increasing temperature.

3. Thermodynamic Modeling Results

As mentioned, in this study the Φ-γ method was used for ther-

Table 3. Henry's law constants and the constants of Arrhenius equation for ethylene absorption in NMP/water system

T (K)	x_w	K_H (bar)	H_0 (bar)	ΔH (kJ/mol)	−TΔS (kJ/mol)	ΔG (kJ/mol)	Ref.
278.20		163.81			20.99	11.68	
298.20	0.011	187.27	8735.1	−9.31	22.50	13.19	This work
328.20		299.31			24.76	15.45	
298.15	0	135.60	-	-	-	-	[43]
	0.083	159.60					
	0.194	202.70					
	0.277	248.20					
298.15	0	127.64	-	-			[45]
298.15	0	136.76	3640.9	−8.14	20.33	12.19	[46]
323.15	0	176.30			22.03	13.89	
343.15	0	210.70			23.39	15.25	
273.15	0	98.90	5014.1	−8.80	19.35	10.55	[47]
278.15	0	108.60			19.70	10.90	
283.15	0	117.31			20.05	11.25	
288.15	0	128.30			20.41	11.61	
278.15	0.104	135.34	-	-	-	-	[44]
	0.241	178.60					
	0.378	298.53					
293.15	0.104	161.30	-	-	-	-	
	0.241	209.50					
	0.378	349.20					

modynamic modeling. For the gas phase, PR-EOS was used, and for the liquid phase the UNIQUAC activity coefficient model was used. The results of this modeling and optimized binary interaction parameters for the ethylene-NMP system are presented in Table 4. The absolute average deviation obtained from the modeling results and experimental solubility data was obtained from 2.76 to 11.03% at different temperatures. The values of τ_{12} and τ_{21} were also adjusted from 0.07 to 0.67.

Fig. 8 shows a comparison of the experimental solubility and the modeling results at different operating conditions. Based on this graph, a reasonable and appropriate agreement was observed between these values.

Fig. 9 demonstrates the sensitivity of the thermodynamic model to the variation of binary interaction parameters of UNIQUAC activ-

Table 4. Comparison of the experimental data and the modeling results including optimized values of the binary interaction parameters in UNIQUAC activity model

T (K)	P_{eq} (bar)	x_{exp}	x_{mod}	τ_{12}	τ_{21}	%AAD
328.2	11.96	0.0550	0.0397	0.32	0.55	11.03
	9.66	0.0378	0.0323			
	7.12	0.0239	0.024			
	5.30	0.0185	0.018			
	3.58	0.0102	0.0122			
	2.00	0.0068	0.0068			
298.2	12.26	0.0603	0.0613	0.07	0.67	2.76
	9.62	0.0486	0.0488			
	6.95	0.0363	0.0357			
	5.18	0.0288	0.0269			
	3.44	0.0185	0.018			
	1.94	0.0099	0.0102			
278.2	12.04	0.0904	0.0747	0.39	0.40	8.80
	9.51	0.0594	0.0593			
	6.89	0.0432	0.0432			
	5.13	0.0307	0.0323			
	3.44	0.0181	0.0217			
	1.86	0.0131	0.0118			

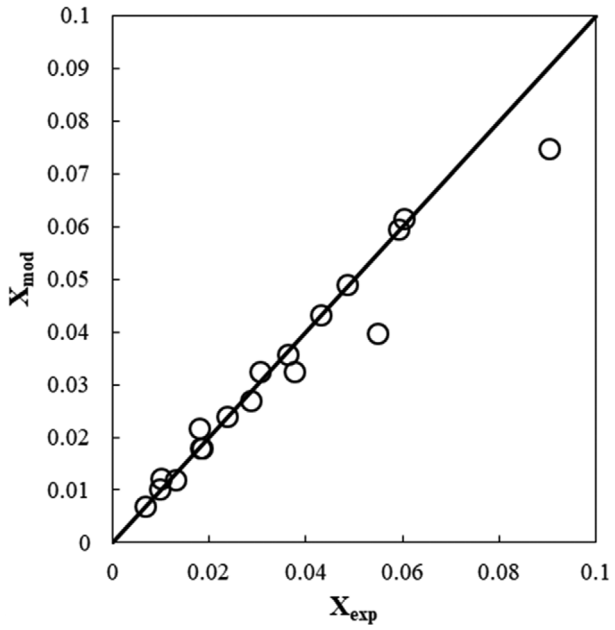

Fig. 8. Prediction of ethylene solubility in NMP using PR-EOS and UNIQUAC equations.

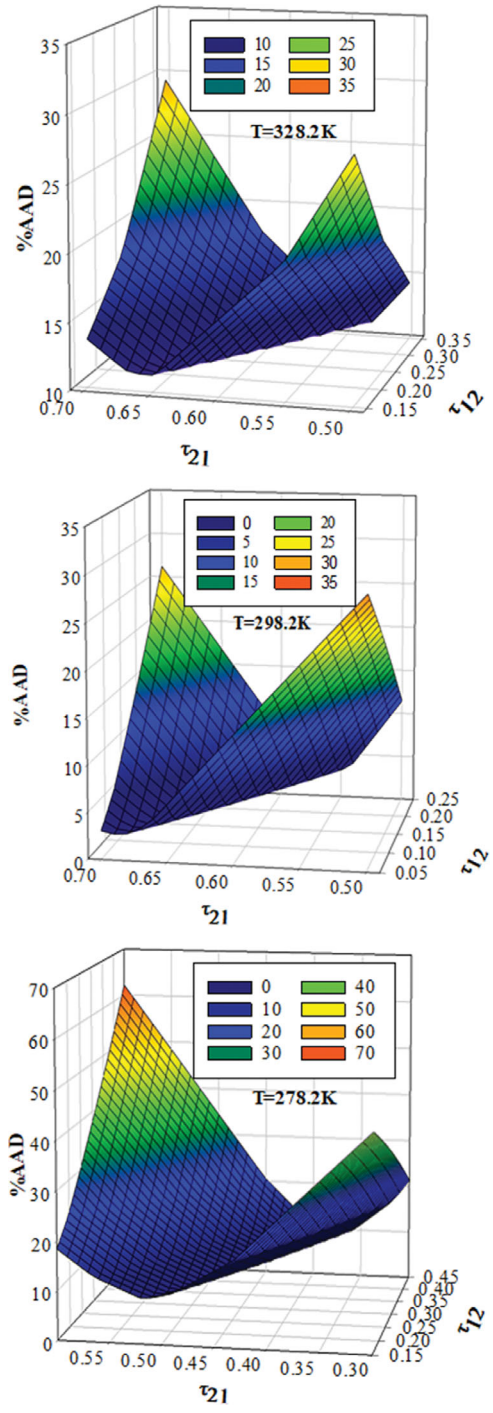

Fig. 9. The effect of binary interaction parameters on the prediction of solubility data of ethylene in NMP at different temperatures.

ity coefficient model. In this figure, the values of the resulting A.A.D. were drawn in relation to different values of the binary interaction parameters at 278.2, 298.2 and 328.2 K. In Fig. 9, for the sake of clarity, only the values representing the error below 30% for 328.2 K, and 30% for 298.2 K, and 70% for 278.2 K are illustrated. The minimum regions of these curves show the optimal range of the binary interaction parameters, which were previously reported in Table 4. According to the calculations, by neglecting the binary interaction parameters in the model (τ_{ij}=0), about 100% error was obtained. This highlights the importance of these parameters in computing, especially in commercial software.

CONCLUSION

Ethylene absorption was performed in a batch stirred vessel using NMP as solvent and the following important conclusions were obtained:

- Physical absorption occurred in these experiments.
- Absorption was faster at higher temperature. At higher pressure this result was more obvious.
- More solubility of ethylene in NMP was obtained at higher pressure and lower temperature.
- The Arrhenius type model was compatible with the experimental data for Henry's law constant calculation to show its dependence on temperature.
- Increasing the temperature increases Henry's law constant.
- PR-EOS and UNIQUAC activity coefficient model was implemented to predict the solubility of ethylene in NMP using Φ-γ approach.
- The optimized values of τ_{12}, τ_{21} in UNIQUAC activity coefficient model were calculated using a trial and error based algorithm.
- Experimental data and thermodynamic modeling results had an acceptable agreement (less than 11% deviation) when the appropriate values of the binary interaction parameters were used.

ACKNOWLEDGEMENT

This paper was prepared from a Ph.D. thesis conducted in the Department of Chemical Engineering, Mahshahr branch, Islamic Azad University, Mahshahr, Iran.

NOMENCLATURE

AAD : absolute average deviation [dimensionless]
E : activity energy [kJ/mole]
EOS : equation of state
G : gibbs free energy [kJ/mole]
H : enthalpy [kJ/mole]
K_H : Henry's law constant [bar]
M_w : molecular weight [g/mol]
n moles (dimensionless)
NMP : N-methyl-2-pyrrolidone
P : pressure [bar]
PR : peng robinson
q : relative molecular area
r : relative molecular volume
R : gas constants [cm^3·bar/mol·K]
S : entropy [kJ/mole·K]
T : temperature [K]
UNIQUAC : universal quasichemical
V : volume [ml]
x : solubility or mole fraction in liquid phase [dimensionless]
y : mole fraction in gas phase [dimensionless]
Z : compressibility factor [dimensionless]

Greek Letter

ω : acentric factor [dimensionless]
ρ : density [g/cm^3]
Φ : fugacity coefficient [dimensionless]
γ : activity coefficient [dimensionless]
τ : binary interaction parameters of UNIQUAC equation [dimensionless]

Subscripts and Superscripts

1 : initial
c : critical
exp : experimental
eq : equilibrium
f : final
g : gas
i : component i
j : component j
mod : model prediction
r : reduced
s : solvent
sat : saturation
t : total

SUPPORTING INFORMATION

Additional information as noted in the text. This information is available via the Internet at http://www.springer.com/chemistry/journal/11814.

REFERENCES

1. Y. Pan, C. Jia, B. Liu, Z. Zhang, X. Tong, H. Li, Z. Li, R. Ssebadduka, C. Sun and L. Yang, *Fluid Phase Equilib.*, **414**, 14 (2016).
2. K.-S. Liao, S. Japip, J.-Y. Lai and T.-S. Chung, *J. Membr. Sci.*, **534**, 92 (2017).
3. M. Manteghian, S. M. M. Safavi and A. Mohammadi, *Chem. Eng. J.*, **217**, 379 (2013).
4. R. B. Eldridge, *Ind. Eng. Chem. Res.*, **32**, 2208 (1993).
5. Y. Wang, Z. Hu, Y. Cheng and D. Zhao, *Ind. Eng. Chem. Res.*, **56**, 4508 (2017).
6. S. Azizi, H. T. Dezfuli, A. Kargari and S. M. Peyghambarzadeh, *Fluid Phase Equilib.*, **387**, 190 (2015).
7. S. Wang, X. Li, H. Wu, Z. Tian, Q. Xin, G. He, D. Peng, S. Chen, Y. Yin and Z. Jiang, *Energy Environ. Sci.*, **9**, 1863 (2016).
8. T. A. Reine and R. B. Eldridge, *Ind. Eng. Chem. Res.*, **44**, 7505 (2005).
9. Z. Bao, G. Chang, H. Xing, R. Krishna, Q. Ren and B. Chen, *Energy*

Environ. Sci., **9**, 3612 (2016).
10. A. Malakhov, S. Bazhenov, V. Vasilevsky, I. Borisov, A. Ovcharova, A. Bildyukevich, V. Volkov, L. Giorno and A. Volkov, *Sep. Purif. Technol.*, **219**, 64 (2019).
11. J. Chmelař, K. Smolná, K. Haškovcová, M. Podivinská, J. Maršálek and J. Kosek, *Polymer*, **59**, 270 (2015).
12. L. Moura, W. Darwich, C. C. Santini and M. F. C. Gomes, *Chem. Eng. J.*, **280**, 755 (2015).
13. H. Mortaheb, M. Mafi, B. Mokhtarani, A. Sharifi, M. Mirzaei, N. Khodapanah and F. Ghaemmaghami, *Chem. Eng. J.*, **158**, 384 (2010).
14. A. Shariati, L. J. Florusse and C. J. Peters, *Fluid Phase Equilib.*, **387**, 143 (2015).
15. Y. Sato, N. Hosaka, H. Inomata and K. Kanaka, *Fluid Phase Equilib.*, **344**, 112 (2013).
16. L.-s. Lee, H.-j. Ou and H.-l. Hsu, *Fluid Phase Equilib.*, **231**, 221 (2005).
17. I. H. Cho, H. K. Yasuda and T. R. Marrero, *J. Chem. Eng. Data*, **40**, 107 (1995).
18. J. Dojcansky, S. Bafroncova and J. Surovy, *Chem. Pap.*, **55**, 71 (2001).
19. K. Nagahama, I. Suzuki and M. Hirata, *J. Chem. Eng. Japan*, **4**, 1 (1971).
20. A. J. Cancelas, M. A. Plata, M. A. Bashir, M. Bartke, V. Monteil and T. F. McKenna, *Macromol. Chem. Phys.*, **219**, 1700565 (2018).
21. S. Kumar and M. K. Mondal, *Korean J. Chem. Eng.*, **35**, 1335 (2018).
22. A. Dashti, F. Zargari, H. R. Harami, A. H. Mohammadi and Z. Nikfarjam, *Korean J. Chem. Eng.*, **36**, 1637 (2019).
23. A. Kitagishi, S. Takizawa, Y. Sato and H. Inomata, *Fluid Phase Equilib.*, **492**, 110 (2019).
24. Y. Mi, C. Yao, S. Zhao and G. Chen, *Chem. Eng. Process.-Process Intensification*, **137**, 137 (2019).
25. J. M. Smith, H. C. Van Ness and M. M. Abbott, *Introduction to chemical engineering thermodynamics*, 7th Ed., Mc-Graw-Hill, Boston (2005).
26. E. W. Washburn, *Chemistry and technology,* Knovel, New York (2003).
27. M. Bohloul, M. A. Sadeghabadi, S. M. Peyghambarzadeh and M. Dehghani, *Fluid Phase Equilib.*, **447**, 132 (2017).
28. M. Bohloul, A. Vatani and S. M. Peyghambarzadeh, *Fluid Phase Equilib.*, **365**, 106 (2014).
29. S. Azizi, S. M. Peyghambarzadeh, M. Saremi and H. Tahmasebi, *Heat Mass Transfer.*, **50**, 1699 (2014).
30. H. Roeentan, S. Azizi, G. Bakeri and S. M. Peyghambarzadeh, *Chem. Eng. Res. Design*, **117**, 240 (2017).
31. J.-N. Jaubert and F. Mutelet, *Fluid Phase Equilib.*, **224**, 285 (2004).
32. S. Oba, S. Suzuki, H. Tanaka, K. Nagahama and M. Hirata, *J. Jpn. Pet. Inst.*, **28**, 202 (1985).
33. I. Polishuk, J. Wisniak and H. Segura, *Chem. Eng. Sci.*, **55**, 5705 (2000).
34. G. Wibawa, M. F. Nafi, A. Permatasari and A. Mustain, *Modern Appl. Sci.*, **9**, 177 (2015).
35. S.-E. K. Fateen, M. M. Khalil and A. O. Elnabawy, *J. Adv. Res.*, **4**, 137 (2013).
36. X. Pu, L. Wu and Y. Liu, *Int. J. Chem. Eng. Appl.*, **8**, 92 (2017).
37. J. M. Prausnitz, R. N. Lichtenthaler and E. G. Azevedo, *Molecular thermodynamics of fluid phase equilibria*, Pearson Education, London (1999).
38. S. Brelvi, *Ind. Eng. Chem. Process Design Dev.*, **21**, 367 (1982).
39. A. Farajnezhad, O. A. Afshar, M. A. Khansary, S. Shirazian and M. Ghadiri, *Fluid Phase Equilib.*, **417**, 181 (2016).
40. B. E. Poling, J. M. Prausnitz and J. P. O'connell, *The properties of gases and liquids*, Mcgraw-Hill, New York (2001).
41. S. Skjold-Jorgensen, B. Kolbe, J. Gmehling and P. Rasmussen, *Ind. Eng. Chem. Process Design Dev.*, **18**, 714 (1979).
42. H. Svensson, C. Hulteberg and H. T. Karlsson, *Int. J. Greenhouse Gas Control*, **17**, 89 (2013).
43. Z. Wu, S. Zeck and H. Knapp, *Berichte der Bunsengesellschaft für Physikalische Chemie*, **89**, 1009 (1985).
44. E. R. Shenderei and F. P. Ivanovskii, *Khim Prom*, **10**, 91 (1963).
45. H. Renon, J. Y. Lenoir and P. Renault, *J. Chem. Eng. Data*, **16**, 340 (1971).
46. S. Shakhova, Y. P. Zubchenko and L. Kaplan, *Khim Prom*, **49**, 108 (1973).
47. E. R. Shenderei and F. P. Ivanovskii, *Gazov. Prom.*, **7**, 11 (1962).